



The H_0 Tension and Late Time Phenomena in $f(T, \mathcal{T})$ Gravity Framework: Role of H_0 Priors

L.K. Duchaniya ^{1,*} and B. Mishra ^{1,†}

¹*Department of Mathematics, Birla Institute of Technology and Science-Pilani, Hyderabad Campus, Hyderabad-500078, India.*

Abstract: In this paper, we have investigated the role of H_0 priors in describing H_0 tension and late-time cosmic behavior of the Universe in the framework of $f(T, \mathcal{T})$ gravity. The specific functional form of $f(T, \mathcal{T})$, where T and \mathcal{T} respectively denote the torsion scalar and trace of the energy-momentum tensor, has the potential to show the H_0 tension and late-time accelerating behavior. The model parameter space has been obtained using multiple cosmological data sets such as cosmic chronometers (CC), Supernovae Type Ia PAN^+ & $SH0ES$, and baryon acoustic oscillations (BAOs). Also, we have incorporated the H_0 priors from the Tip of the Red Giant Branch (TRGB) and HW. The analysis shows the ability of the model to replicate comparative performance with the standard Λ CDM model through AIC and BIC. From the results obtained, it has been observed that the inclusion of the BAO data set shifts the H_0 values lower as compared to that of the $CC + PAN^+$ & $SH0ES$ data set, whereas the combination of HW prior favors higher H_0 values. This demonstrates the sensitivity of the model to different H_0 priors. The findings indicate that the $f(T, \mathcal{T})$ gravity model can provide an alternative approach to show cosmological tension and late-time cosmic phenomena.

I. INTRODUCTION

The late-time cosmic behavior of the Universe has emerged as the most compelling enigmas in contemporary cosmology. Following an extended period of almost uniform expansion, observational evidence revealed that an unidentified energy component is driving spacetime expansion at an accelerating rate [1, 2]. The leading candidate for this phenomenon is dark energy (DE) [3, 4], which has a major share of approximately 70% of the total mass-energy of the Universe. As a consequence, it largely influences the ultimate fate of the Universe. The discovery of cosmic acceleration poses profound questions about our understanding of gravity and drives new investigations into the fundamental principles of physics. The Λ CDM model that describes the Universe as a composition of cold dark matter (CDM) and DE represented by a cosmological constant Λ has been corroborated by several cosmological observations [5–10]. However, the discrepancies in Hubble constant H_0 and structure growth parameter S_8 pose additional challenges. The recent observed values of H_0 show a notable rift between the value derived from early Universe observations such as cosmic microwave background (CMB) via the Planck satellite [11] and gleaned from local measurements utilizing Cepheid variables and Supernovae Type Ia [12]. In particular, Riess et al. [12] within the SH0ES Team have reported a Hubble constant estimate of $73.30 \pm 1.04 \text{ km s}^{-1} \text{ Mpc}^{-1}$, based on Supernovae Type Ia observations. Whereas the H0LiCOW Collaboration [13] derived a value of $73.3^{+1.7}_{-1.8} \text{ km s}^{-1} \text{ Mpc}^{-1}$ through a strong gravitational lensing of quasars. Further, Freedman et al. [14] reported a lower estimate of $69.8 \pm 1.9 \text{ km s}^{-1} \text{ Mpc}^{-1}$, obtained using the tip of the red giant branch (TRGB) as a distance indicator. The Planck Collaboration [15] provides a Hubble constant value of $67.4 \pm 0.5 \text{ km s}^{-1} \text{ Mpc}^{-1}$, while Aboot et al. [16] suggest $67.2^{+1.2}_{-1.0} \text{ km s}^{-1} \text{ Mpc}^{-1}$. This divergence between the estimates from early and late Universe measurements, known as the H_0 tension, raises significant questions in modern cosmology. Initially identified with the first release of Planck data [11], the H_0 tension has garnered increasing scrutiny and attention in recent studies [15, 17, 18]. This ongoing inconsistency has led to exploring possible modifications to the standard cosmological model and considering new physics beyond Λ CDM.

General relativity (GR) encapsulates the interplay between matter, energy, and the curvature of spacetime. However, modifications in GR have been inevitable to address the late-time behavior of the Universe. A simple approach to understanding this phenomenon is introducing the cosmological constant, leading to the Λ CDM model. Otherwise, GR can be refined by integrating extra terms or scalar fields into the gravitational action. These modifications may include higher-order curvature invariants or scalar fields coupled to the curvature. This may provide a robust

* duchaniya98@gmail.com

† bivu@hyderabad.bits-pilani.ac.in

theoretical framework that accommodates a concordance model for cosmology through various straightforward adjustments [19, 20]. The modifications can be incorporated as the Einstein-Hilbert action [21, 22] to provide various cosmological phenomena. One such gravitational modification is the torsional equivalent formulation of GR, known as the Teleparallel Equivalent of GR (TEGR) [23, 24]. TEGR permits the formulation of second-order equations in four-dimensional spacetime and employs the Weitzenböck connection [25]. This framework is characterized by four linearly independent tetrad fields, which serve as the orthonormal bases for the tangent space at each point in spacetime, with the torsion tensor being derived from the first derivatives of these tetrads. To note, $f(R)$ gravity [21] presents the basic modification of GR, whereas $f(T)$ [26–33] gravity is the modification of TEGR. Further, many variations of the torsion-influenced gravitational theory such as $f(T, T_G)$ (T_G refers to the Gauss-Bonnet term) [34, 35], $f(T, B)$ [36, 37] (B signifies the boundary term), $f(T, \phi)$ [38–41] (ϕ represents the scalar field), and $f(T, \mathcal{T})$ [42–47] gravity have been proposed.

The H_0 tension refers to the observed discrepancies in the Hubble constant measurements in various observational methodologies, which challenges the standard Λ CDM model [48–54]. The motivation of this study is to examine the influence of H_0 priors on the H_0 tension and late time behavior of the Universe in $f(T, \mathcal{T})$ gravitational theory [42]. Within this framework, the gravitational Lagrangian can be developed using the torsion scalar T functions and the trace of the energy-momentum tensor \mathcal{T} .

The paper is organized as follows: In Sec.-II, we present a brief overview of the mathematical formalism of $f(T, \mathcal{T})$ gravity. The formalism of the cosmological data sets and the mathematical formalism of the statistical criteria for model comparison (AIC and BIC) is defined in Sec.-III. In Sec.-IV, we analyze the cosmological observations for different data set combinations and the H_0 priors. In addition, we obtain the best-fit values of the model parameters. In Sec.-V, we present the evolution of the background cosmological parameters to analyze the behavior of the model at late times. We summarize the results of cosmological observation for the Λ CDM model in the appendix and give a conclusion on the findings in Sec.-VI.

II. MATHEMATICAL FORMALISM

In teleparallel gravity (TG), the tetrad fields e_μ^A act as dynamical variables in place of the usual metric tensor $g_{\mu\nu}$ in GR. The metric tensor in TG can be represented as,

$$g_{\mu\nu} = \eta_{AB} e_\mu^A e_\nu^B. \quad (1)$$

The Greek indices denote space-time coordinates, while the capital Latin indices indicate tangent space-time coordinates. η_{AB} denotes the Minkowski space-time and the tetrad fields satisfy the orthogonality condition $e^\mu_A e^B_\mu = \delta^B_A$. Employing the Weitzenböck connection as a framework for $f(T, \mathcal{T})$ gravity, we can define

$$\hat{\Gamma}^\lambda_{\nu\mu} \equiv e^\lambda_A (\partial_\mu e^A_\nu + \omega^A_{B\mu} e^B_\nu), \quad (2)$$

where $\omega^A_{B\mu}$ represents a flat spin connection that guarantees invariance under Lorentz transformations, which stems directly from the indices of the tangent space. On the other hand, the spin connections used in GR are not flat [55] because they depend on the tetrads. In TG, the equations governing motion incorporate both gravitational and local degrees of freedom, depicted by the pair of tetrads and spin connections. Now, the torsion tensor characterized by the anti-symmetric part of the Weitzenböck connection can be described as,

$$T^\lambda_{\mu\nu} \equiv \hat{\Gamma}^\lambda_{\nu\mu} - \hat{\Gamma}^\lambda_{\mu\nu} = e^\lambda_A \partial_\mu e^A_\nu - e^\lambda_A \partial_\nu e^A_\mu. \quad (3)$$

The torsion tensor exhibits covariance under diffeomorphisms and Lorentz transformations. Provided that the torsion tensor has been correctly contracted, the torsion scalar can be represented as,

$$T \equiv \frac{1}{4} T^{\rho\mu\nu} T_{\rho\mu\nu} + \frac{1}{2} T^{\rho\mu\nu} T_{\nu\mu\rho} - T_{\rho\mu}{}^\rho T^{\nu\mu}{}_\nu. \quad (4)$$

The action in TG is based on the teleparallel Lagrangian T and the $f(T)$ gravity extends this Lagrangian to an arbitrary function $f(T)$. The action of $f(T, \mathcal{T})$ gravity [42] is,

$$S = \frac{1}{16\pi G} \int d^4x e [T + f(T, \mathcal{T}) + \mathcal{L}_m], \quad (5)$$

where T is the torsion scalar, \mathcal{T} be trace of the energy-momentum tensor, \mathcal{L}_m denotes matter Lagrangian and G represents the gravitational constant. The determinant of the tetrad field is expressed as $e = \det[e^A_\mu] = \sqrt{-g}$. Varying action (5) with respect to the tetrad field, one can obtain the gravitational field equations for $f(T, \mathcal{T})$ gravity as,

$$\begin{aligned} & [e^{-1}\partial_\mu(ee^\rho_A S_\rho^{\mu\nu}) - e^\lambda_A T^\rho_{\mu\lambda} S_\rho^{\nu\mu}](1 + f_T) + e^\rho_A S_\rho^{\mu\nu} [\partial_\mu(T)f_{TT} + \partial_\mu(\mathcal{T})f_{T\mathcal{T}}] + \frac{1}{4}e^\nu_A [T + f(T)] \\ & - f_{\mathcal{T}} \left(\frac{e^\rho_A T_\rho^\nu + pe^\rho_A}{2} \right) = 4\pi G e^\rho_A T_\rho^\nu. \end{aligned} \quad (6)$$

For brevity, we denote $f_T = \frac{\partial f}{\partial T}$, $f_{TT} = \frac{\partial^2 f}{\partial T^2}$, $f_{\mathcal{T}} = \frac{\partial f}{\partial \mathcal{T}}$ and $f_{T\mathcal{T}} = \frac{\partial^2 f}{\partial T \partial \mathcal{T}}$. The total energy-momentum tensor can be represented as T_ρ^ν . The superpotential, $S_\rho^{\mu\nu} \equiv \frac{1}{2}(K^{\mu\nu}_\rho + \delta_\rho^\mu T^{\alpha\nu}_\alpha - \delta_\rho^\nu T^{\alpha\mu}_\alpha)$. The contortion tensor in the superpotential can be defined as, $K^{\mu\nu}_\rho \equiv \frac{1}{2}(T^{\nu\mu}_\rho + T_\rho^{\mu\nu} - T^{\mu\nu}_\rho)$.

We consider the homogeneous and isotropic flat Friedmann-Lemaître-Robertson-Walker (FLRW) space-time as,

$$ds^2 = dt^2 - a^2(t)[dx^2 + dy^2 + dz^2], \quad (7)$$

where $a(t)$ denotes the scale factor that represents the rate of expansion in the spatial dimensions. From Eq. (4), the torsion scalar can be derived as,

$$T = -6H^2 \quad (8)$$

and the associated tetrad field can be expressed as $e^A_\mu \equiv \text{diag}(1, a(t), a(t), a(t))$. We can now derive the field equations for $f(T, \mathcal{T})$ gravity Eq. (6) as,

$$3H^2 = 8\pi G \rho_m - \frac{1}{2}(f + 12H^2 f_T) + f_{\mathcal{T}}(\rho_m + p_m), \quad (9)$$

$$\dot{H} = -4\pi G(\rho_m + p_m) - \dot{H}(f_T - 12H^2 f_{TT}) - H(\dot{\rho}_m - 3\dot{p}_m)f_{T\mathcal{T}} - f_{\mathcal{T}} \left(\frac{\rho_m + p_m}{2} \right). \quad (10)$$

An over dot represents ordinary derivative with respect to cosmic time t . The trace of the energy-momentum tensor, $\mathcal{T} = \rho_m - 3p_m$, where p_m denotes the matter pressure and ρ_m be the corresponding energy density term. The Friedmann Eqs.(9-10) can be written as,

$$3H^2 = 8\pi G(\rho_m + \rho_{DE}), \quad (11)$$

$$-\dot{H} = 4\pi G(\rho_m + p_m + \rho_{DE} + p_{DE}). \quad (12)$$

From Eqs. (9-12), the energy density (ρ_{DE}) and pressure (p_{DE}) for the DE component can be retrieved as,

$$\rho_{DE} \equiv -\frac{1}{16\pi G} [f + 12H^2 f_T - 2f_{\mathcal{T}}(\rho_m + p_m)], \quad (13)$$

$$p_{DE} \equiv (\rho_m + p_m) \left[\frac{1 + \frac{f_{\mathcal{T}}}{8\pi G}}{1 + f_T - 12H^2 f_{TT} + H \frac{d\rho_m}{dH} (1 - 3c_s^2)} f_{T\mathcal{T}} - 1 \right] + \frac{1}{16\pi G} [f + 12H^2 f_T - 2f_{\mathcal{T}}(\rho_m + p_m)]. \quad (14)$$

The behavior of total EoS parameter (ω_{tot}) and the deceleration parameter (q) are significant to analyze the late time behavior of the Universe, which can be expressed as,

$$\omega_{tot} = \frac{p_m + p_{DE}}{\rho_m + \rho_{DE}} \equiv -1 - \frac{2\dot{H}}{3H^2}, \quad (15)$$

$$q = \frac{1}{2}(1 + 3\omega_{tot}). \quad (16)$$

III. COSMOLOGICAL OBSERVATION DATA SETS

We have presented brief descriptions of the cosmological data sets and the methodology used to obtain the best-fit values of the cosmological parameters. The best-fit values of the parameters will enable us to study the late-time behavior of the Universe along with the H_0 tension, if any. The data sets to be used are Hubble data, Supernovae Type Ia data, and BAOs. The H_0 priors used are Red Giant Branch (TRGB) and HW. We shall use the PYTHON package chain consumer Ref [56] to execute a Markov Chain Monte Carlo (MCMC) analysis to integrate these data sets. MCMC is a robust sampling technique that extracts samples from the posterior distribution of the cosmological model. This method is widely used in Bayesian statistics to estimate model parameters and quantify uncertainties. In this process, a large sample size would be required to ensure the accuracy of the model. We compute the one-dimensional parameter distribution that provides the posterior distribution of each parameter and the two-dimensional parameter distributions which will reveal the covariance relationship between pairs of parameters. Our analysis culminates in generating MCMC corner plots at 1σ and 2σ confidence level.

Cosmic Chronometers (CC): We employed 31 data points for the Hubble parameter derived from the cosmic chronometer (CC) methodology. This technique allows for directly analyzing the Hubble function across a range of redshifts up to $z \leq 2$. The strength of CC data lies in its ability to evaluate the age difference between two passively evolving galaxies that formed simultaneously but have a small difference in redshift, enabling the calculation of $\frac{\Delta z}{\Delta t}$. Refs [57–64] provide the basis for the CC data points. The associated estimate for χ_H^2 is given as,

$$\chi_H^2(\Theta) = \sum_{i=1}^{31} \frac{(H(z_i, \Theta) - H_{\text{obs}}(z_i))^2}{\sigma_H^2(z_i)}, \quad (17)$$

the Hubble parameters can be divided into two categories: $H(z_i, \Theta)$ indicates the theoretical values of the Hubble parameter at a given redshift z_i whereas $H_{\text{obs}}(z_i)$ refers to the observed values of the Hubble parameter at z_i , along with an observational uncertainty denoted by $\sigma_H(z_i)$.

Supernovae Type Ia data set (SNIa) : This data set for our MCMC analysis includes the Type Ia supernova collection, which incorporates 1701 Supernovae data points that represent relative luminosity distances within the redshift interval $0.01 < z < 2.3$ [12, 65, 66]. SNIa data sets were used for this study as Pantheon+ [PAN^+ & $SHOES$]. The distance modulus is the discrepancy between the apparent magnitude m and the absolute magnitude M . At a redshift z_i , the distance modulus function $\mu(z_i, \Theta)$ can be formulated as

$$\mu(z_i, \Theta) = m - M = 5 \log_{10} [D_L(z_i, \Theta)] + 25, \quad (18)$$

the luminosity distance $D_L(z_i, \Theta)$ can be formulated as

$$D_L(z_i, \Theta) = c(1 + z_i) \int_0^{z_i} \frac{dz'}{H(z', \Theta)}, \quad (19)$$

where c indicates the speed of the light. To determine the chi-square (χ_{SN}^2) value with the PAN^+ & $SHOES$ compilation, which includes 1701 Supernovae data points, we apply the following formula[67]:

$$\chi_{\text{SN}}^2 = (\Delta\mu(z_i, \Theta))^T C^{-1} (\Delta\mu(z_i, \Theta)). \quad (20)$$

In this context, C refers to the covariance matrix incorporating systematic and statistical uncertainties in the measurements. Additionally, $\Delta\mu(z_i, \Theta) = \mu(z_i, \Theta) - \mu(z_i)_{\text{obs}}$ indicates the disparity between the predicted and observed distance modulus at the redshift z_i .

BAO data set: We also analyze a combined baryon acoustic oscillation (BAO) data set of distinct data points. For this study, we utilize a BAO data set that features observations from the Six-degree Field Galaxy Survey at an effective redshift of $z_{\text{eff}} = 0.106$ [68], the BOSS DR11 quasar Lyman-alpha measurements at $z_{\text{eff}} = 2.4$ [69], and the SDSS Main Galaxy Sample at $z_{\text{eff}} = 0.15$ [70]. Additionally, we incorporate measurements of $H(z)$ and angular diameter distances obtained from the SDSS-IV eBOSS DR14 quasar survey at effective redshifts $z_{\text{eff}} = \{0.98, 1.23, 1.52, 1.94\}$ [71], along with the consensus BAO measurements of the Hubble parameter and the corresponding comoving angular diameter distances from SDSS-III BOSS DR12 at $z_{\text{eff}} = \{0.38, 0.51, 0.61\}$ [5]. Our analysis considers the complete

covariance matrix for the sets of BAO data. To evaluate the BAO data set for the cosmological model, it is necessary to establish the Hubble distance $D_H(z)$, the comoving angular diameter distance $D_M(z)$, and the volume-average distance $D_V(z)$.

$$D_H(z) = \frac{c}{H(z)}, \quad D_M(z) = (1+z)D_A(z), \quad D_V(z) = \left[(1+z)^2 D_A^2(z) \frac{z}{H(z)} \right]^{1/3}, \quad (21)$$

where $D_A(z) = (1+z)^{-2}D_L(z)$ denotes the angular diameter distance. To include the BAO findings in MCMC analyses, we need to take into account the pertinent combinations of parameters:

$$\mathcal{F}(z_i) = \left\{ \frac{D_V(z_i)}{r_s(z_d)}, \frac{r_s(z_d)}{D_V(z_i)}, D_H(z_i), D_M(z_i) \left(\frac{r_{s,\text{fid}}(z_d)}{r_s(z_d)} \right), H(z_i) \left(\frac{r_s(z_d)}{r_{s,\text{fid}}(z_d)} \right), D_A(z_i) \left(\frac{r_{s,\text{fid}}(z_d)}{r_s(z_d)} \right) \right\}, \quad (22)$$

where $r_s(z_d)$ represents the sound horizon at the drag epoch, while $r_{s,\text{fid}}(z_d)$ indicates the fiducial sound horizon. To accomplish this, we calculated the comoving sound horizon $r_s(z)$ at the redshift $z_d \approx 1059.94$ [15], which corresponds to the conclusion of the baryon drag epoch.

$$r_s(z) = \int_z^\infty \frac{c_s(\tilde{z})}{H(\tilde{z})} d\tilde{z} = \frac{1}{\sqrt{3}} \int_0^{1/(1+z)} \frac{da}{a^2 H(a) \sqrt{1 + \left[\frac{3\Omega_{b,0}}{4\Omega_{\gamma,0}} \right] a}}, \quad (23)$$

where the subsequent values are utilized: $\Omega_{b,0} = 0.02242$ [15], $T_0 = 2.7255$ K [72], and a reference value of $r_{s,\text{fid}}(z_d) = 147.78$ Mpc. The relevant estimate for χ_{BAO}^2 is given by [67].

$$\chi_{\text{BAO}}^2(\Theta) = (\Delta\mathcal{F}(z_i, \Theta))^T C_{\text{BAO}}^{-1} \Delta\mathcal{F}(z_i, \Theta), \quad (24)$$

where C_{BAO} denotes the covariance matrix for the chosen BAO data, and $\Delta\mathcal{F}(z_i, \Theta) = \mathcal{F}(z_i, \Theta) - \mathcal{F}_{\text{obs}}(z_i)$ indicates the discrepancy between the theoretical and measured values of \mathcal{F} at redshift z_i .

We will investigate how an H_0 prior affects the selected functional form $f(T, \mathcal{T})$ along with the previously described data set. The measurement from the H0LiCOW Collaboration, based on strong lensing of quasars, yields a value of $H_0 = 73.3_{-1.8}^{+1.7}$ km s⁻¹ Mpc⁻¹ HW [13]. The measurement using the tip of the red giant branch (TRGB) as a standard candle with $H_0 = 69.8 \pm 1.9$ km s⁻¹ Mpc⁻¹ [14].

The HW measurement usually refers to a recent high-value local estimation of the Hubble constant, H_0 , provided by the H0LiCOW collaboration. This estimation is grounded in observations of Cepheid variable stars and Supernovae Type Ia in the nearby galaxies, which act as standard candles to determine distances to galaxies and thus measure the expansion rate of the Universe. The TRGB offers an independent determination of the Hubble constant. This approach depends on measuring the brightness of red giant stars in nearby galaxies. The TRGB technique enables accurate distance assessments of galaxies, which can be used to compute H_0 .

The Λ CDM model acts as a foundational framework for comprehending cosmic evolution. When comparing other cosmological models to the Λ CDM model, the Akaike Information Criterion (AIC) and the Bayesian Information Criterion (BIC) are vital tools for selecting models. The AIC can be expressed as,

$$\text{AIC} = -2 \ln L_{\text{max}} + 2k, \quad (25)$$

where k indicates the number of parameters used in the estimation procedure and L_{max} is the maximum value of the likelihood function. The BIC can be given as,

$$\text{BIC} = -2 \ln L_{\text{max}} + k \ln \mu, \quad (26)$$

The sample size of the observational data combination is denoted by μ . AIC and BIC serve as valuable tools for determining whether a new cosmological model significantly improves upon the fit to the data compared to Λ CDM model. Additionally, if the value of the ΔAIC or ΔBIC is lower, we can say that the chosen cosmological model is similar to the standard Λ CDM model. This comparison helps us understand the need to introduce new cosmic phenomena or modify the established model. The ΔAIC or ΔBIC can be defined as,

$$\Delta\text{AIC} = \text{AIC}_{\text{model}} - \text{AIC}_{\Lambda\text{CDM}}, \quad (27)$$

$$\Delta\text{BIC} = \text{BIC}_{\text{model}} - \text{BIC}_{\Lambda\text{CDM}}. \quad (28)$$

IV. COSMOLOGICAL MODEL

In the Friedmann equations [Eq.(9)-Eq.(10)], we need to incorporate some well-motivated functional form of $f(T, \mathcal{T})$. The selection of the functional form for $f(T, \mathcal{T})$ is vital in the sense that it influences the predictions of the model and its alignment with observational data. We may also investigate possible variations from Λ CDM that analyze the late-time cosmic acceleration and some direction to address the H_0 tension. In this setting, we have considered the following form of $f(T, \mathcal{T})$ [42],

$$f(T, \mathcal{T}) = \alpha T^n \mathcal{T} + \Lambda, \quad (29)$$

where $\alpha \neq 0$, $n \neq 0$ and Λ are arbitrary constants. At present, one can express the Friedmann Eq. (9) as,

$$\alpha = \frac{2 - 2\Omega_{m0} + \frac{\Lambda}{3H_0^2}}{(1 + 2n)\Omega_{m0}(-6H_0^2)^{-n}}, \quad (30)$$

where H_0 and Ω_{m0} respectively represent the Hubble parameter and matter density parameter at present time. From Eq. (30), it can be inferred that the model parameter α depends on other parameters such as H_0 , Ω_{m0} , n and Λ . Therefore, we will constrain these parameters using the cosmological data sets. By defining the dimensionless Hubble parameter $E(z) = \frac{H(z)}{H_0}$, the Friedmann Eq. (9) for this model can be reformulated as

$$E^2(z) = (1 + z)^3 \Omega_{m0} - \frac{\Lambda}{6H_0^2} + \left(1 - \Omega_{m0} + \frac{\Lambda}{6H_0^2}\right) (1 + z)^3 E^{2n}(z). \quad (31)$$

To ensure that the term $\frac{\Lambda}{6H_0^2}$ remains dimensionless, we define the cosmological constant as $\Lambda = p H_0^2$ with p is a parameter without dimensions. This reformulation expresses the cosmological constant about the Hubble parameter, allowing p to reflect the effect of DE on the expansion of the Universe while maintaining consistency in units within the equation. Now, Eq. (31) becomes,

$$E^2(z) = (1 + z)^3 \Omega_{m0} - \frac{p}{6} + \left(1 - \Omega_{m0} + \frac{p}{6}\right) (1 + z)^3 E^{2n}(z). \quad (32)$$

Eq. (32) is an implicit formulation for $E(z)$. Considering that analytical solutions for Eq. (32) are impractical, we have adhered to the numerical methods to compute the parameters. The methodology used as described in Sec.-III and the results obtained are described below.

In Fig.-1, we have presented the 1σ and 2σ confidence levels along with the posterior distributions for the parameters H_0 , Ω_{m0} , p , n and M using CC, PAN^+ & $SH0ES$ and BAO data sets in addition to the TRGB and HW priors. It displays the marginalized posterior distributions for different combinations of parameters. The inner contours indicate the 68% confidence level while the outer contours represent the 95% confidence level. This visual representation facilitates a thorough evaluation of parameter uncertainties and correlations. In Table-I, the exact value of the model parameters along with the nuisance parameter M are given. It can be seen that the highest H_0 value is recorded for the data set combination CC+ PAN^+ & $SH0ES$ +HW i.e., $H_0 = 72.69^{+0.88}_{-0.85} \text{ km s}^{-1} \text{ Mpc}^{-1}$. This indicates that the inclusion of H_0 prior has a significant effect on value of H_0 . At the same time, the lowest H_0 value obtained to be $H_0 = 69.25^{+0.62}_{-0.64} \text{ km s}^{-1} \text{ Mpc}^{-1}$ from the combination of CC+ PAN^+ & $SH0ES$ +BAO data sets. This indicates that the inclusion of BAO data lowering H_0 and diminishes the effect of H_0 prior. Interestingly, when BAO data is analyzed with HW prior, the H_0 value increases again. The resultant value of H_0 remains between [71-72] for the combined data sets CC+ PAN^+ & $SH0ES$ with H_0 with HW and TRGB priors. The inclusion of the BAO data set shows the range of H_0 between [69-70]. The BAO data imposes a limiting influence on H_0 that favors lower values. This can likely be attributed to the inherent characteristics of the BAO measurements, which are responsive to the sound horizon scale and the expansion rate across various redshifts. Consequently, BAO data typically adjusts H_0 estimates to values that portray a slower late-time cosmic expansion than those derived from local measurements or priors like HW and TRGB. Thus, integrating BAO data in the combination significantly lowers H_0 , presenting a notable contrast to the higher values that the local data set suggests. The HW prior elevates H_0 to greater values, while the TRGB prior decreases it.

We have also computed the AIC and BIC values, which will provide a statistical foundation for selecting the appropriate model. Results related to the Λ CDM model can be found in the Appendix, particularly in Table-IV. Lower values of Δ AIC and Δ BIC suggest that the model using the chosen data sets closely resembles the Λ CDM model, indicating enhanced performance. In this study, the Δ AIC and Δ BIC values for the data set combinations CC+PAN⁺&SH0ES incorporating H_0 priors are significantly lower than those for the CC+PAN⁺&SH0ES+BAO combinations that also include H_0 priors. This implies that the combination of CC+PAN⁺&SH0ES with H_0 priors alone performs better than when BAO data is part of the combination. The decreased Δ AIC and Δ BIC values for the CC+PAN⁺&SH0ES with H_0 priors signify that this particular data combination aligns more closely with the standard Λ CDM model.

Table I: The best fit values of the parameters explored by MCMC analysis. The first column enumerates a combination of data sets with the H_0 priors. The second column presents the constrained H_0 values. The third column contains the constrained Ω_{m0} values. The fourth and fifth columns represent the optimal p and n values respectively. The sixth column provides the nuisance parameter M .

Data set	H_0 [km s ⁻¹ Mpc ⁻¹]	Ω_{m0}	p	n	M
CC+PAN ⁺ &SH0ES	$72.56^{+0.98}_{-1.01}$	$0.377^{+0.055}_{-0.069}$	$-0.5^{+2.5}_{-0.0}$	$-2.25^{+0.34}_{-0.46}$	$-19.260^{+0.031}_{-0.028}$
CC+PAN ⁺ &SH0ES+TRGB	$71.98^{+0.86}_{-0.90}$	$0.378^{+0.055}_{-0.069}$	$-0.405^{+2.381}_{-0.084}$	$-2.23^{+0.33}_{-0.46}$	$-19.276^{+0.025}_{-0.026}$
CC+PAN ⁺ &SH0ES+HW	$72.69^{+0.88}_{-0.85}$	$0.370^{+0.057}_{-0.064}$	$-0.44^{+2.35}_{-0.34}$	$-2.24^{+0.31}_{-0.48}$	$-19.257^{+0.027}_{-0.023}$
CC+PAN ⁺ &SH0ES+BAO	$69.25^{+0.62}_{-0.64}$	$0.286^{+0.021}_{-0.020}$	$-0.5^{+2.1}_{-0.0}$	-2.06 ± 0.18	-19.361 ± 0.017
CC+PAN ⁺ &SH0ES+BAO+TRGB	$69.30^{+0.64}_{-0.56}$	$0.286^{+0.021}_{-0.020}$	$-0.39^{+1.99}_{-0.10}$	-2.07 ± 0.18	$-19.360^{+0.017}_{-0.016}$
CC+PAN ⁺ &SH0ES+BAO+HW	$69.78^{+0.58}_{-0.63}$	$0.282^{+0.021}_{-0.020}$	$-0.8^{+2.1}_{-0.0}$	$-2.12^{+0.20}_{-0.18}$	$-19.348^{+0.016}_{-0.017}$

Table II: The statistical comparison between the chosen model and the standard Λ CDM model. Details regarding the Λ CDM model are given in Appendix. The first column enumerates the data sets including the H_0 priors. The second column displays the values of χ^2_{\min} . The third and fourth column respectively provides the value of AIC and BIC. The fifth and sixth column respectively illustrates the values of Δ AIC and Δ BIC.

data set	χ^2_{\min}	AIC	BIC	Δ AIC	Δ BIC
CC+PAN ⁺ &SH0ES	1538.23	1548.23	1554.42	3.01	5.49
CC+PAN ⁺ &SH0ES+TRGB	1539.94	1549.94	1556.13	2.76	5.24
CC+PAN ⁺ &SH0ES+HW	1538.37	1548.37	1554.57	3.08	5.57
CC+PAN ⁺ &SH0ES+BAO	1570.62	1580.62	1586.83	7.45	9.93
CC+PAN ⁺ &SH0ES+BAO+TRGB	1570.73	1580.73	1586.95	7.23	9.73
CC+PAN ⁺ &SH0ES+BAO+HW	1575.41	1585.41	1591.63	10.6	13.11

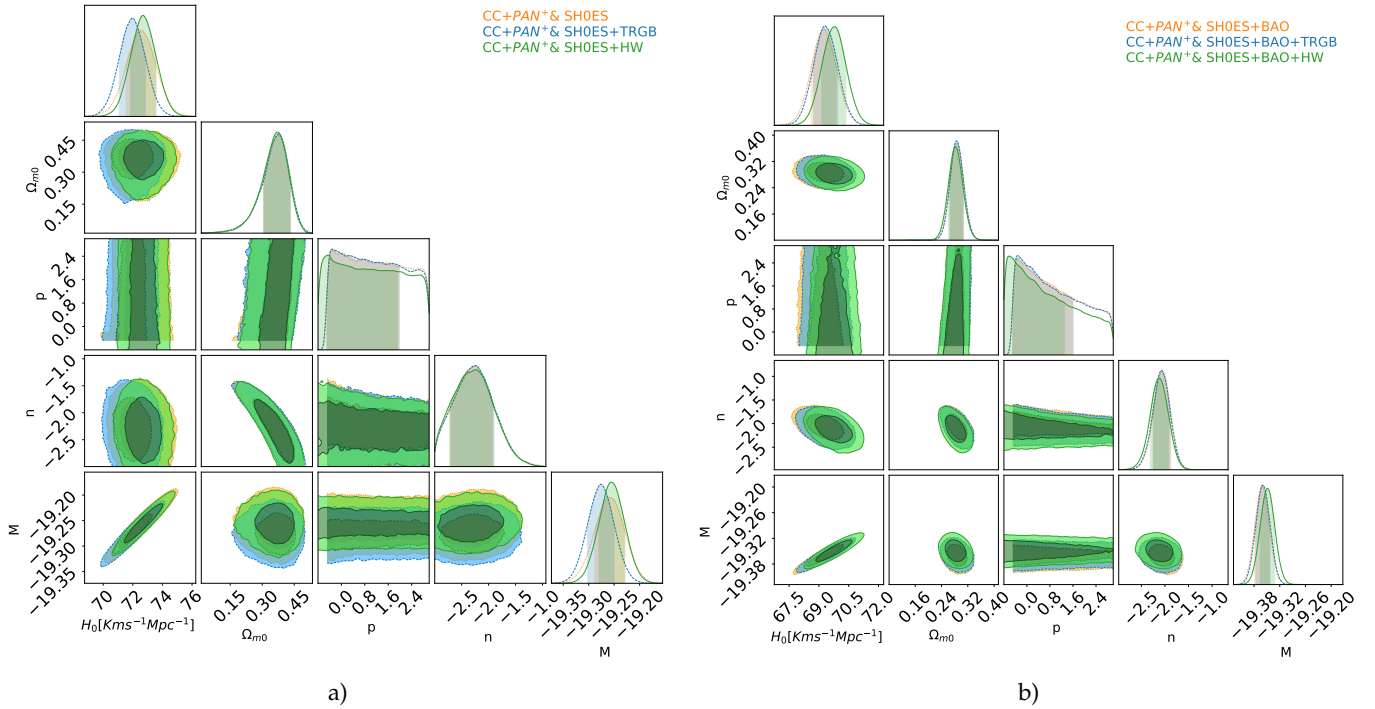


Figure 1: The contour plot of 1σ and 2σ uncertainty regions and posterior distribution for the model parameters with the combination of data sets (a) CC, PAN⁺&SHOES (b) CC, PAN⁺&SHOES and BAO. The H_0 priors are: TRGB (Blue) and HW (Green).

V. DYNAMICS OF COSMOLOGICAL PARAMETERS

In this section, we shall analyze the background cosmological parameters to explore the late time behavior for the $f(T, \mathcal{T})$ model. Also, we compare these findings with those from the standard Λ CDM model. In Fig.-2a, we have shown the behavior of the Hubble parameter for different combinations of data sets with prior and compared to that of Λ CDM model. It has been observed that the curves are traversing in a similar fashion to that of Λ CDM model and well within the error bars. So, the model can effectively reproduce the Λ CDM behavior. To illustrate the discrepancies between the chosen model and the conventional Λ CDM model, we introduce the relative difference,

$$\Delta_r H(z) = \frac{|H_{\text{model}} - H_{\Lambda\text{CDM}}|}{H_{\Lambda\text{CDM}}}. \quad (33)$$

The evolutionary behavior of the relative difference has been shown in Fig.-2b. Fig.-3 illustrates the progression of the Hubble parameter and the relative difference in the Hubble parameter for the CC, PAN⁺&SHOES and BAO data set that includes the H_0 priors. This progression closely resembles the pattern depicted in Fig.-2, which shows almost uniform behavior across the data sets.

In Fig.-4a, we present the progression of the distance modulus for the chosen model in comparison to the Λ CDM model using 1701 data points from the PAN⁺&SHOES data set. The selected model shows a significant agreement with the Λ CDM model. The relative difference

$$\Delta_r \mu(z) = \frac{|\mu_{\text{model}} - \mu_{\Lambda\text{CDM}}|}{\mu_{\Lambda\text{CDM}}}. \quad (34)$$

In Fig.-4b, we depict the comparative evolution of the distance modulus between the chosen model and the Λ CDM model, In Fig.-5, we illustrate the evolution of the distance modulus function and the relative difference distance modulus function for the CC, PAN⁺&SHOES, and BAO data set, while incorporating H_0 priors. This trend closely aligns with the pattern observed in Fig.-4, which shows consistent behavior among the data sets.

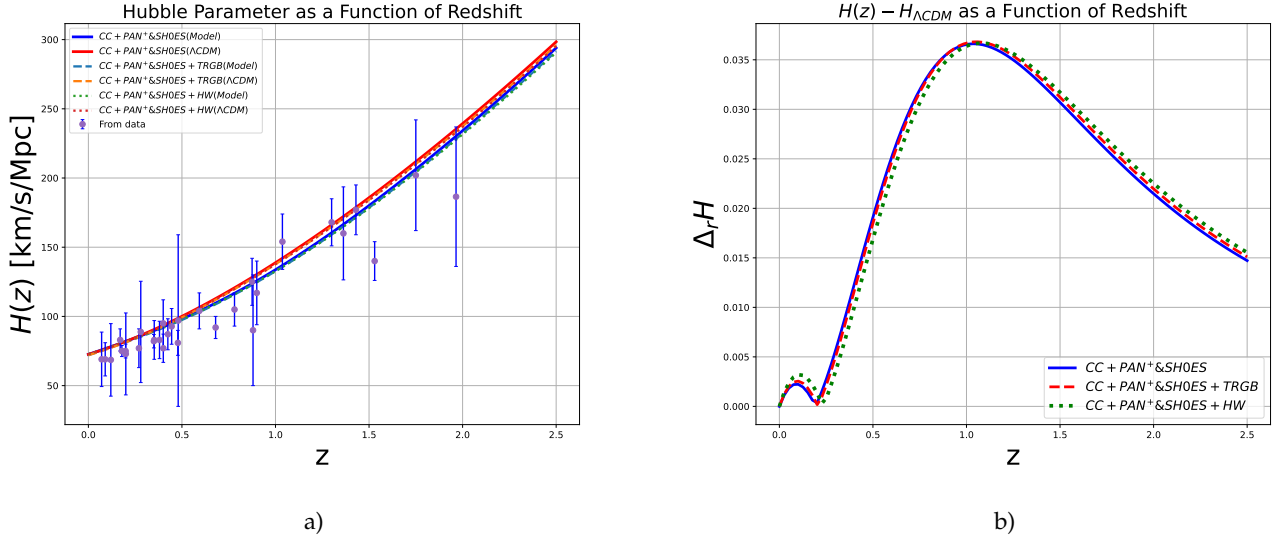


Figure 2: (a) Evolutionary behavior of Hubble parameter and Λ CDM model in redshift (b) Relative variation between the Hubble parameter and Λ CDM model. The combination of data sets: $CC, PAN^+ \& SHOES$. The H_0 priors are: TRGB and HW

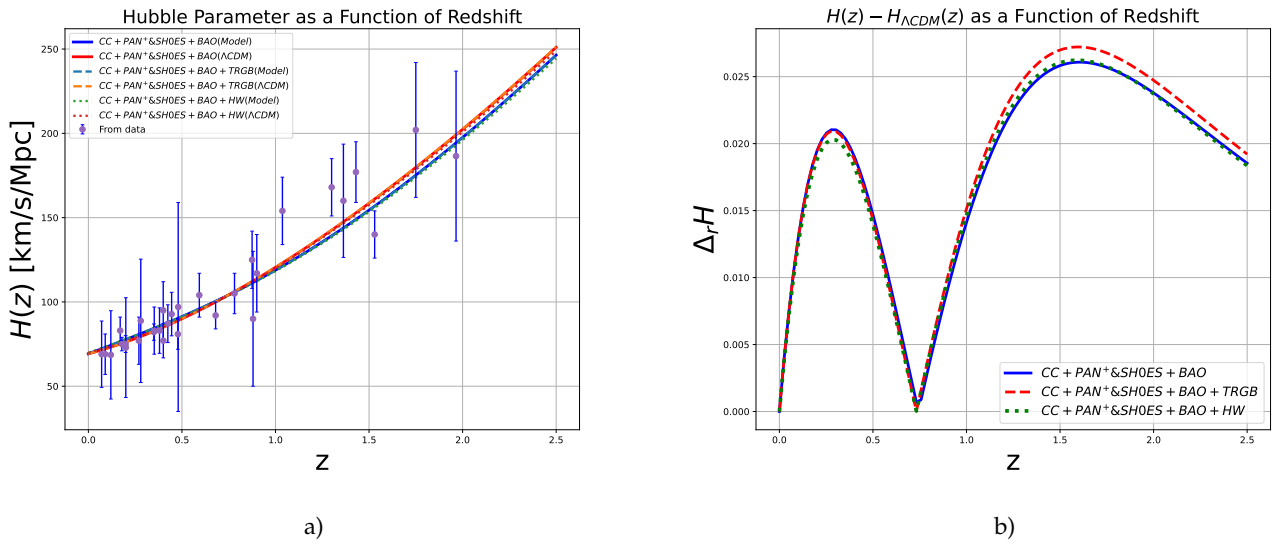


Figure 3: (a) Evolutionary behavior of Hubble parameter and Λ CDM model in redshift (b) Relative variation between the Hubble parameter and Λ CDM model. The combination of data sets: $CC, PAN^+ \& SHOES$ and BAO. The H_0 priors are: TRGB and HW

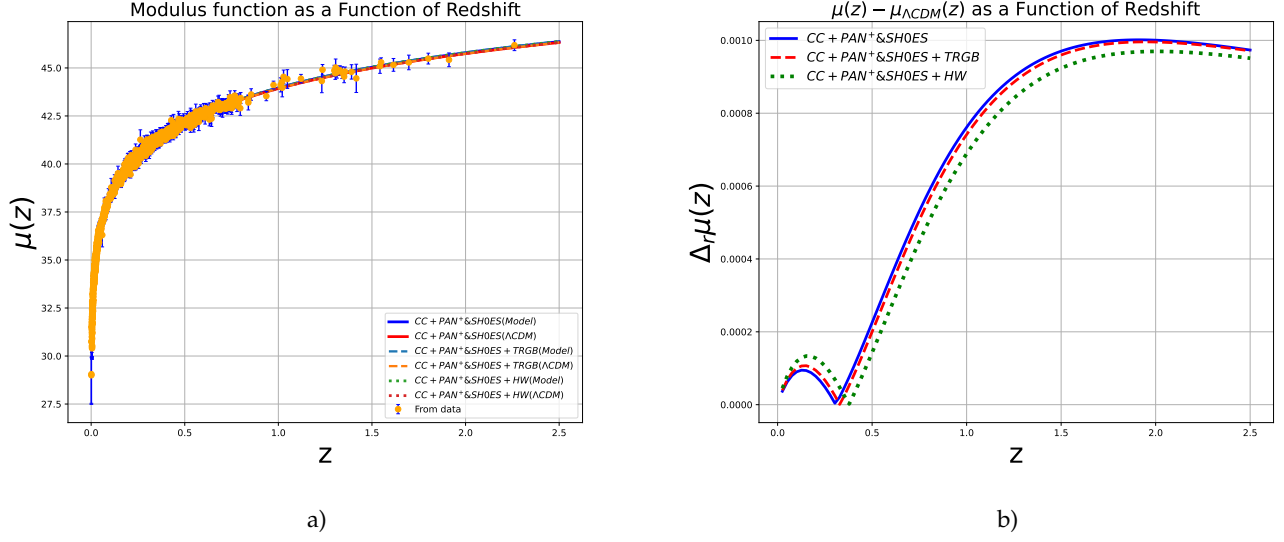


Figure 4: (a) Evolutionary behavior of distance modulus and Λ CDM model in redshift (b) Relative variation between the distance modulus and Λ CDM model. The combination of data sets: CC, PAN^+ & $SHOES$. The H_0 priors are: TRGB and HW

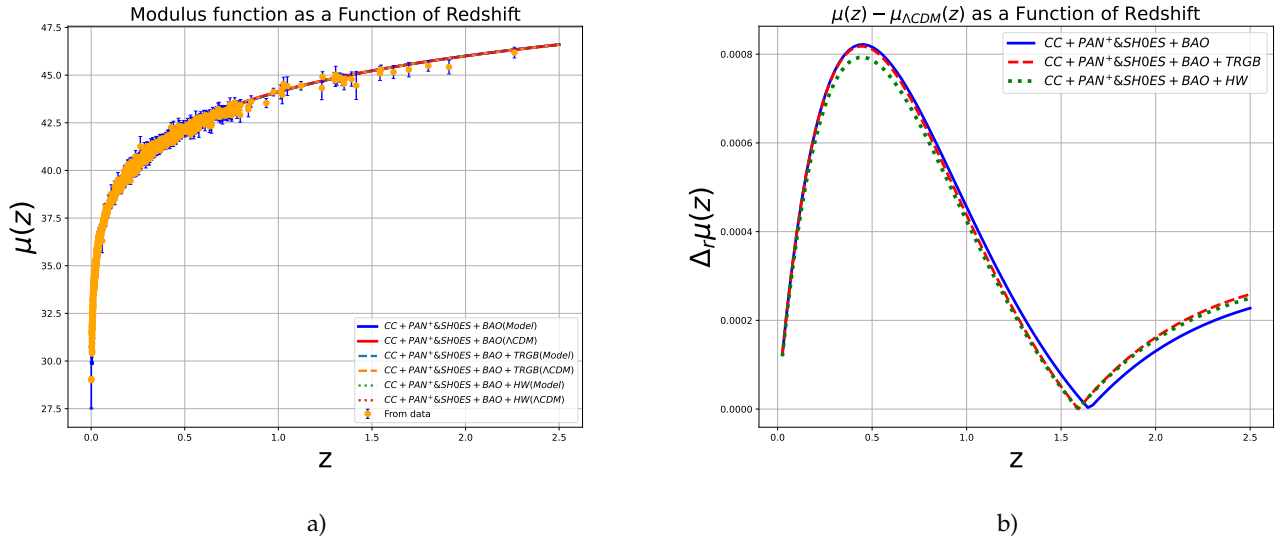


Figure 5: (a) Evolutionary behavior of distance modulus and Λ CDM model in redshift (b) Relative variation between the distance modulus and Λ CDM model. The combination of data sets: CC, PAN^+ & $SHOES$ and BAO. The H_0 priors are: TRGB and HW

The deceleration parameter (q), the total equation of state parameter (ω_{tot}), and the matter-energy density as a function of redshift (z) can be expressed as

$$q = -1 + \frac{(1+z)H'(z)}{H(z)}, \quad (35)$$

$$\omega_{tot} = -1 + \frac{2(1+z)H'(z)}{3H(z)}, \quad (36)$$

$$\Omega_m = \frac{\Omega_{m0}(1+z)^3 H_0^2}{H^2(z)}, \quad (37)$$

In Fig.-6, we show the progression of the deceleration parameter for the chosen model and the Λ CDM model. The chosen model demonstrates the shift from a decelerating phase to an accelerating phase of the Universe, suggesting that it can accurately reflect the accelerated expansion behavior of the Universe. Furthermore, we ascertain the current value of the deceleration parameter. The current value of the deceleration parameter and the transition point for the various data sets are detailed in Table-III. The deceleration parameter is essential for distinguishing between the decelerating and accelerating phases of the Universe. The results from the chosen model regarding the current value of the deceleration parameter and the transition point align with cosmological observations [73, 74].

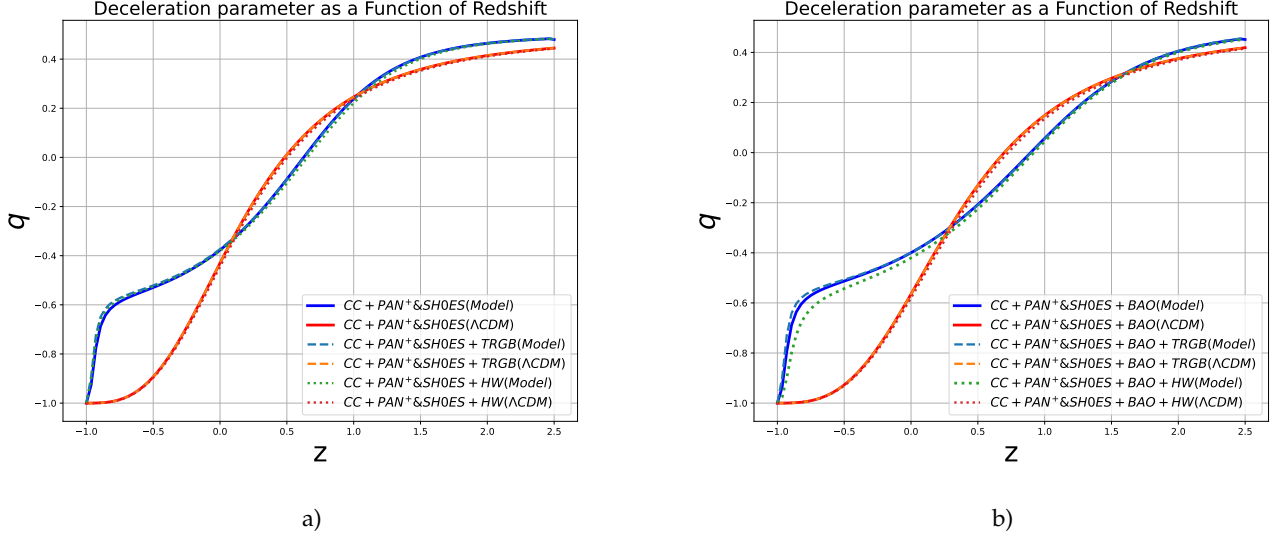


Figure 6: Evolutionary behavior of deceleration parameter and Λ CDM model in redshift with the combination of data sets (a) $CC, PAN^+ \& SH0ES$ (b) $CC, PAN^+ \& SH0ES$ and BAO. The H_0 priors are: TRGB and HW

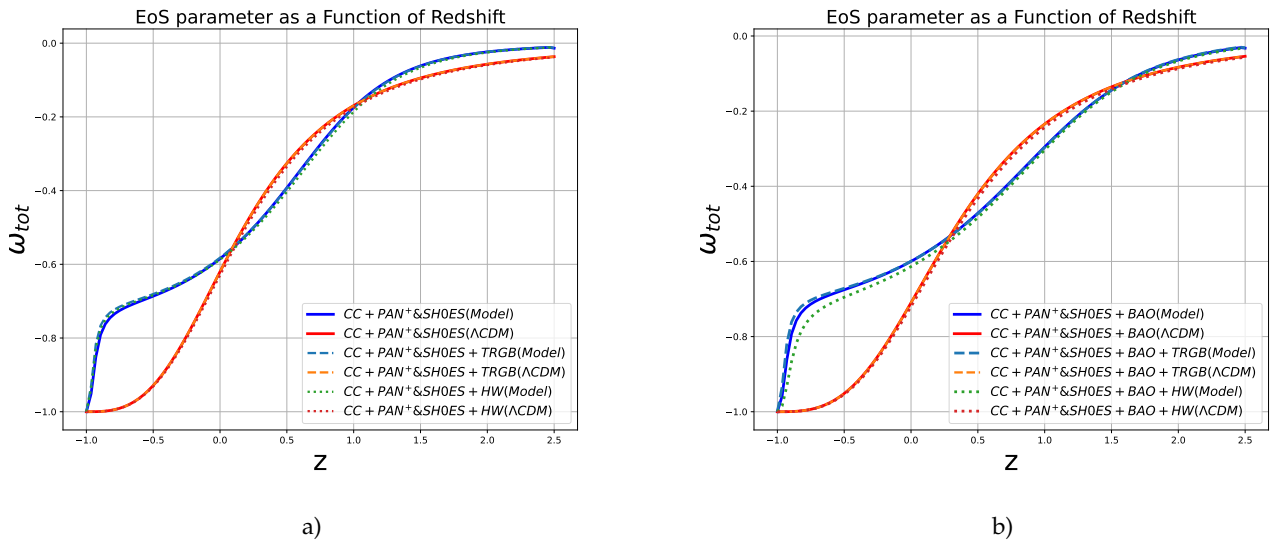


Figure 7: Evolutionary behavior of EoS parameter and Λ CDM model in redshift with the combination of data sets (a) $CC, PAN^+ \& SH0ES$ (b) $CC, PAN^+ \& SH0ES$ and BAO. The H_0 priors are: TRGB and HW

In Fig.-7, we illustrate the progression of the total equation of state (EoS) parameter for the chosen model compared to the Λ CDM model. The EoS parameter indicates a quintessence phase for the Universe as it meets the quintessence criterion $-1 < \omega < -\frac{1}{3}$. This behavior showcases a departure from constant DE, implying that the DE component in the chosen model changes over cosmic time. At later stages, the EoS parameter approaches -1 , confirming the alignment with the Λ CDM model. This tendency to converge towards $\omega = -1$ further reinforces the alignment of the model with observational data at later epochs, demonstrating the quintessence-like behavior in the early Universe and the eventual approach to a cosmological constant in the far future. A summary of the current value of the total EoS parameter is presented in Table-III.

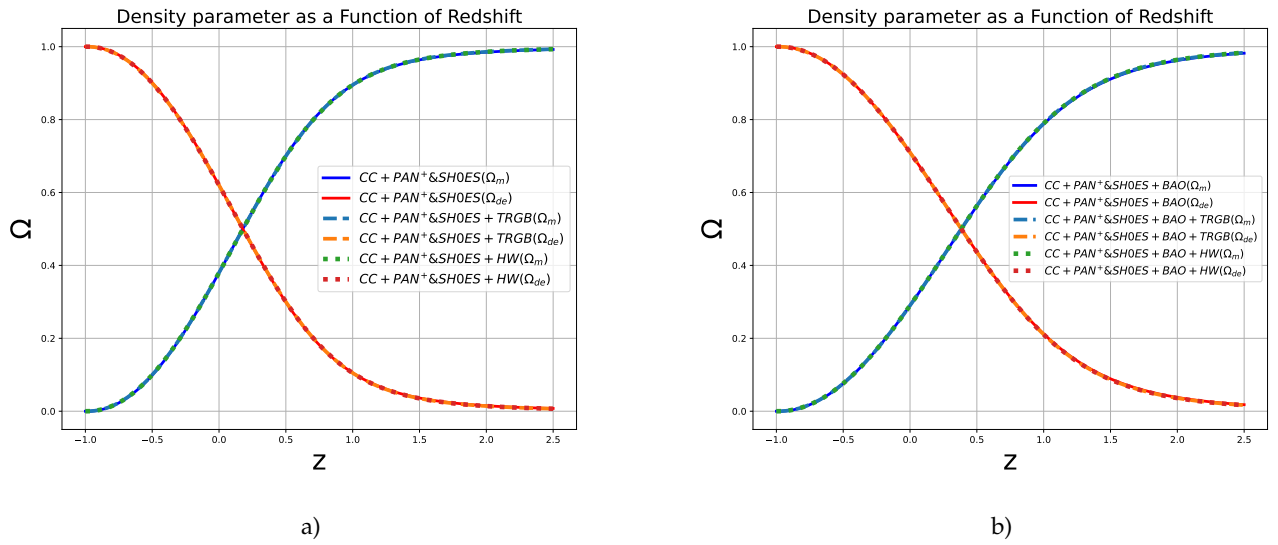


Figure 8: Evolutionary behavior of density parameters in redshift with the combination of data sets (a) CC, PAN+ & SHOES (b) CC, PAN+ & SHOES and BAO. The H_0 priors are: TRGB and HW

In Fig.-8, we show the changes in the density parameters for both matter and DE in the Universe as a function of redshift. This graph illustrates the evolving relationship between matter and DE, indicating that DE density increasingly prevails in later periods, leading to the accelerated expansion of the Universe. The current values of these density parameters are given in Table-III. In the early Universe, dark matter is the primary component of energy density at higher redshifts, greatly exceeding that of DE. As redshift decreases, the share of dark matter diminishes while the impact of DE gradually increases. In the late Universe, DE becomes the dominant factor, and at lower redshifts, it surpasses dark matter and propels the accelerated expansion.

Data set	For $f(T, \mathcal{T})$ model					For the Λ CDM model		
	q_0	ω_0	Transition $z_{transi.}$	Ω_m^0	Ω_{de}^0	q_0	ω_0	Transition $z_{transi.}$
CC+PAN+&SH0ES	-0.374	-0.583	0.62	0.38	0.62	-0.43	-0.62	0.48
CC+PAN+&SH0ES+TRGB	-0.370	-0.58	0.63	0.38	0.62	-0.43	-0.62	0.48
CC+PAN+&SH0ES+HW	-0.379	-0.586	0.65	0.37	0.63	-0.445	-0.63	0.50
CC+PAN+&SH0ES+BAO	-0.399	-0.599	0.89	0.29	0.71	-0.565	-0.71	0.70
CC+PAN+&SH0ES+ BAO+TRGB	-0.398	-0.599	0.90	0.29	0.71	-0.565	-0.71	0.70
CC+PAN+&SH0ES+ BAO+HW	-0.419	-0.613	0.92	0.28	0.72	-0.58	-0.72	0.72

Table III: Present value of the parameters and the transition point. The upper or lower indices 0 represent the current time at $z = 0$.

The $Om(z)$ diagnostic is another approach to differentiate different DE cosmological models. It can be expressed as [75, 76],

$$Om(z) = \frac{E^2(z) - 1}{(1+z)^3 - 1}, \quad (38)$$

evaluating the $Om(z)$ values at varying redshifts can provide information about the properties and behavior of DE. The methodology for two-point difference diagnostics can be outlined as,

$$Om(z_1 - z_2) = Om(z_1) - Om(z_2) \quad (39)$$

If $Om(z_1, z_2) > 0$, then the model indicates the quintessence scenario, whereas for $Om(z_1, z_2) < 0$, it indicates phantom behavior given that $z_1 < z_2$. Also, if $Om(z)$ is consistent across different redshifts, it suggests that DE can be linked to the cosmological constant [75]. We have illustrated the comparison with the model presented here and Λ CDM model in Fig.-9. It can be seen that $Om(z)$ parameter shows stability across the redshift interval $0 < z < 2.5$. Such behavior is essential for grasping the dynamics of the Universe and its accelerated expansion. The slope of $Om(z)$ is a significant indicator of DE models. A positive slope denotes the existence of phantom behavior, characterized by an equation of state parameter $\omega < -1$. In contrast, a negative slope is associated with the quintessence region, where $\omega > -1$.

In Fig.-9, the slope of the $Om(z)$ parameter exhibits a decreasing trend as the redshift increases, indicating that the influence of DE becomes more pronounced over time. This decline suggests a shift in the dynamics of the Universe, reflecting the changing roles of matter and DE as the Universe evolves. This decrease aligns with the quintessence phase of the Universe, where the equation of state parameter ω is greater than -1 . In Fig.-9a, we observed that the slope of $Om(z)$ exhibits an increasing trend beyond the redshift point $z = 1$, indicating that the chosen model is also consistent with a phantom phase of the Universe. In Fig.-9b, the slope of $Om(z)$ stabilizes at a constant value after $z = 1$, suggesting that the chosen model shows a Λ CDM-like behavior.

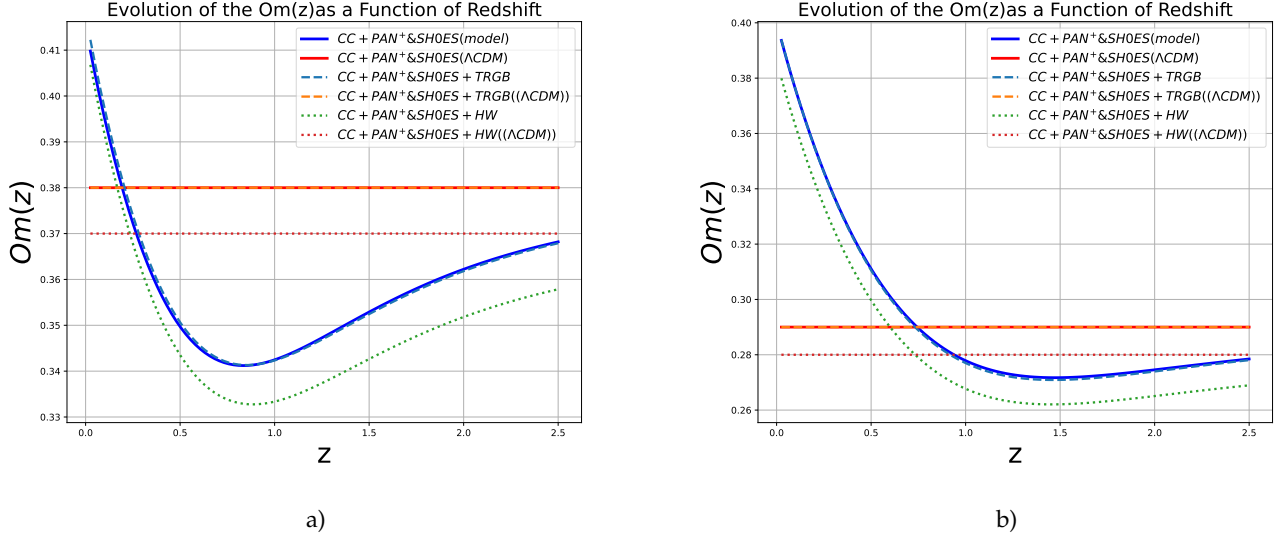


Figure 9: Evolutionary behavior of $Om(z)$ parameter and Λ CDM model in redshift with the combination of data sets (a) CC, PAN⁺&SHOES (b) CC, PAN⁺&SHOES and BAO. The H_0 priors are: TRGB and HW

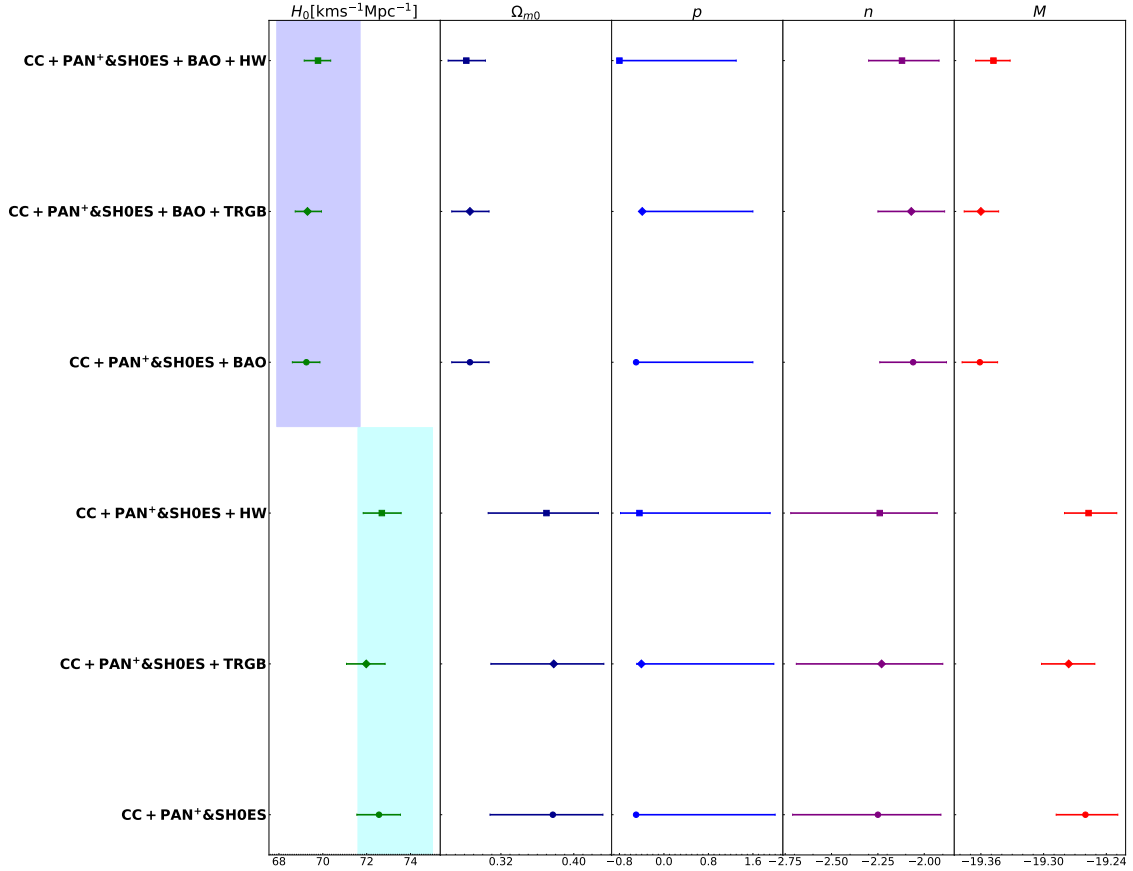


Figure 10: Whisker plot for the chosen $f(T, \mathcal{T})$ framework. This plot provides a visual representation of the distributions of several key parameters: the Hubble constant H_0 , the matter-energy density Ω_{m0} , and the model parameters p and n , along with the nuisance parameter M . In the first column, the blue-shaded region represents the TRGB prior, while the cyan-shaded region indicates the HW prior.

The whisker plot is a comprehensive tool for encapsulating the uncertainties and variability inherent in the parameters under investigation. It provides a clear view of their ranges and central tendencies. By scrutinizing the distribution and median values illustrated in the plot, we can extract valuable insights into the behavior of the chosen model and its alignment with observational cosmology. This comparative analysis elucidates the interactions between different parameters and their influence on the dynamics of the Universe within the framework of $f(T, \mathcal{T})$ theory. In Fig.-10, the whisker plot distinctively delineates parameter values obtained from various data set combinations. We observed a marked discrepancy in the estimates of H_0 and Ω_{m0} across these configurations. For instance, the combination of CC and PAN^+ & $SH0ES$ data set, when utilizing the H_0 priors TRGB and HW, yields H_0 values in the range of 71 to 72. In contrast, integration with the BAO data set results in H_0 values shifting to approximately 69 to 70. This variation underscores the existing H_0 tension, indicating that the chosen model captures this discrepancy effectively. Fig.-10 demonstrates that an increase in the matter component corresponds to a rise in the expansion rate of the Universe, whereas a decrease in the matter component indicates a slower expansion rate of the Universe.

APPENDIX

Presented here are the results of the Λ CDM model. In Fig.- 11, we display the posterior distributions alongside the 1σ and 2σ confidence intervals for various data set combinations, offering an in-depth view of parameter constraints. The detailed results for each combination of data sets are consolidated in Table-IV. This approach underscores the alignment of chosen results with the standard expectations of the Λ CDM framework, enabling a robust evaluation of model performance in the selected data sets.

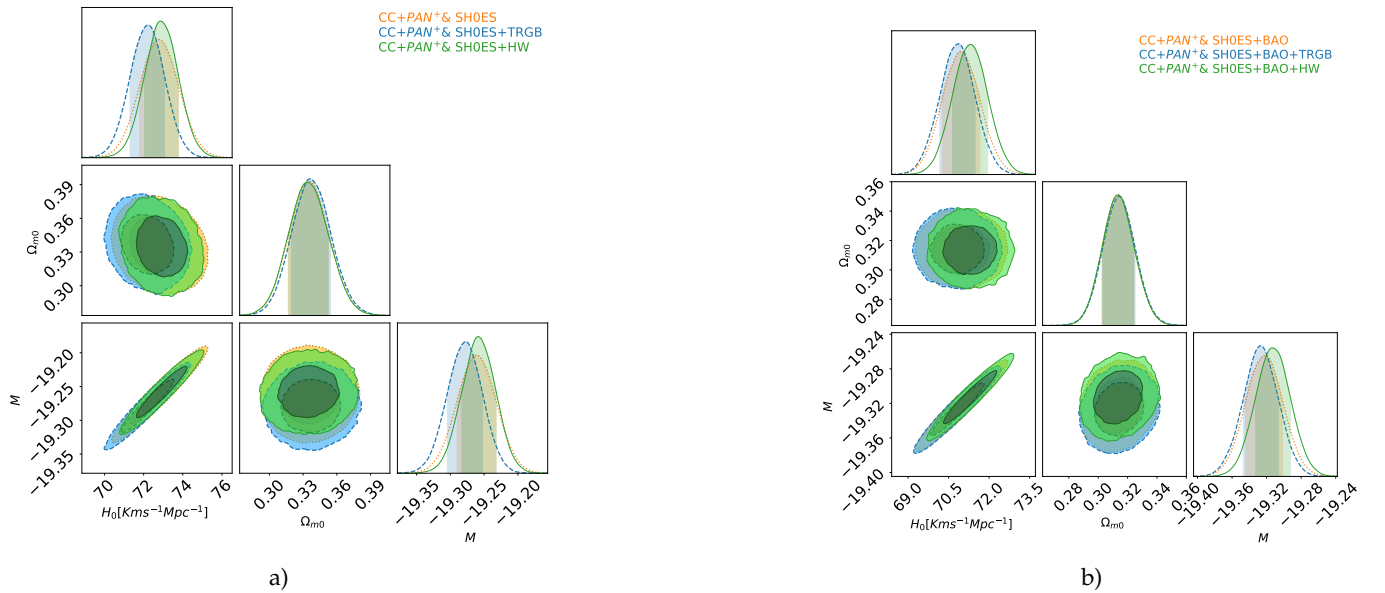


Figure 11: The contour plot of 1σ and 2σ uncertainty regions and posterior distribution for the model parameters with the combination of data sets (a) CC, PAN^+ & $SH0ES$ (b) CC, PAN^+ & $SH0ES$ and BAO. The H_0 priors are: TRGB (Blue) and HW (Green).

Table IV: The results for the Λ CDM model. The first column identifies the data set combinations and the applied H_0 priors. The second and third columns present the derived values for H_0 and $\Omega_{m,0}$, respectively, while the fourth column displays the value of the nuisance parameter. The fifth column provides the minimized χ^2_{min} values, with the sixth and seventh columns showing the AIC and BIC values, respectively.

Λ CDM	H_0	$\Omega_{m,0}$	M	χ^2_{min}	AIC	BIC
CC+PAN ⁺ & SH0ES	$72.81^{+0.96}_{-1.01}$	0.335 ± 0.018	-19.261 ± 0.029	1539.22	1545.22	1548.93
CC+PAN ⁺ & SH0ES+TRGB	$72.24^{+0.82}_{-0.93}$	$0.335^{+0.019}_{-0.016}$	$-19.277^{+0.024}_{-0.028}$	1541.18	1547.18	1550.89
CC+PAN ⁺ & SH0ES+HW	$72.82^{+0.95}_{-0.77}$	$0.333^{+0.019}_{-0.016}$	$-19.258^{+0.026}_{-0.025}$	1539.29	1545.29	1549.00
CC+PAN ⁺ & SH0ES+BAO	$70.93^{+0.72}_{-0.67}$	0.313 ± 0.011	$-19.321^{+0.020}_{-0.023}$	1567.17	1573.17	1576.90
CC+PAN ⁺ & SH0ES+BAO+TRGB	$70.89^{+0.59}_{-0.71}$	$0.315^{+0.010}_{-0.012}$	$-19.327^{+0.021}_{-0.020}$	1567.50	1573.50	1577.22
CC+PAN ⁺ & SH0ES+BAO+HW	$71.32^{+0.62}_{-0.68}$	$0.314^{+0.010}_{-0.011}$	$-19.314^{+0.022}_{-0.019}$	1568.81	1574.81	1578.52

VI. CONCLUSION

We have presented a cosmological model in $f(T, \mathcal{T})$ gravity that provides insight into the H_0 tension and late time behavior. The results obtained in the model for some specific form of the functional $f(T, \mathcal{T})$ have been compared with the standard Λ CDM model. Our analysis aimed at obtaining the best-fit values of the model parameters using the CC, PAN⁺&SH0ES and BAO data sets alongside the H_0 priors TRGB and HW [Table-I]. In the analysis, we have shown the influence of H_0 value on the H_0 priors. Specifically, we assess the impact of H_0 when combined with various data sets. We have also conducted an MCMC analysis for the Λ CDM model, utilizing it as a basis for our statistical evaluation. We have also shown the differences and similarities between the $f(T, \mathcal{T})$ gravity model presented and the established Λ CDM model.

In our analysis, we observe that for the combination of the CC and PAN⁺&SH0ES data set, alongside the H_0 priors TRGB and HW, the value of H_0 tends to shift toward higher values of the Hubble constant. Specifically, for the data set combination CC+PAN⁺&SH0ES+HW, we obtain an elevated H_0 value of $72.69^{+0.88}_{-0.85}$. This upward shift in H_0 highlights the influence of the HW H_0 prior. Conversely, for the data set combination CC+PAN⁺&SH0ES+TRGB, a lower H_0 value of $71.98^{+0.86}_{-0.90}$ is found, illustrating the effect of the TRGB H_0 prior in moderating the Hubble constant. This sensitivity to the choice of H_0 prior underscores its significant impact on the inferred value of the Hubble constant. On the other hand, when we incorporate the BAO data set, the H_0 value shifts to a lower range, likely due to contributions from early-Universe effects. Specifically, after including the BAO data set, the combination of CC+PAN⁺&SH0ES+BAO yields a lower H_0 value than that derived from other data set combinations. This variation in H_0 values exemplifies the phenomenon of the H_0 tension. Notably, chosen $f(T, \mathcal{T})$ model also exhibits this H_0 tension. Including the H_0 priors TRGB and HW within the data set, combinations result in lower and higher shifts in H_0 values, respectively. Fig.-(10) shows that as the matter component increases, the expansion rate of the Universe also rises. In contrast, reducing the matter component leads to a slower Universe expansion rate.

Alternatively, we further investigate our selected $f(T, \mathcal{T})$ model, which presents intriguing features due to its lack of a corresponding Λ CDM limit. Specifically, there is no set of parameter values within this model that replicates the exact behavior of the Λ CDM model. From a statistical perspective, the AIC and BIC values for the data set combination CC+PAN⁺&SH0ES are found to be very close to those of the standard Λ CDM model, suggesting that this data set combination supports the Λ CDM model well. However, when including the BAO data set with CC+PAN⁺&SH0ES, the AIC and BIC values increase compared to the Λ CDM model. This indicates that the CC+PAN⁺&SH0ES+BAO data set combination does not provide strong evidence in favor of the Λ CDM model.

To investigate late-time cosmology, we present the evolution of key background cosmological parameters such as the deceleration parameter, the total EoS parameter, the energy density parameters for matter and DE, and the $Om(z)$

diagnostic parameter for our selected $f(T, \mathcal{T})$ model alongside the standard Λ CDM model. For the data set combination, the current values of deceleration and EoS parameters, as well as the energy density and the deceleration to acceleration transition redshift, are summarized in Table-III.

The behavior of the deceleration parameter indicates that the chosen model captures the transition from early Universe deceleration to late time acceleration. The behavior of the EoS parameter supports the quintessence-like behavior at the late phase of the evolution. The energy density parameters indicate a shift from a matter-dominated early Universe to a DE dominated late-time phase. So, the model can describe the late time cosmic phenomena of the Universe.

Finally, the approach presented to study the H_0 tension and late time behavior of the Universe in $f(T, \mathcal{T})$ gravity framework may provide some basis for further study. In particular, the study can be integrated with the Cosmic Microwave Background (CMB) data from surveys such as the Planck mission. We anticipate a deeper understanding of inflationary dynamics and other key phenomena in the early Universe and this may provide a new avenue to analyze the fundamental properties of cosmic evolution.

ACKNOWLEDGEMENTS

LKD acknowledges the financial support provided by University Grants Commission (UGC) through Senior Research Fellowship UGC Ref. No.: 191620180688 to carry out the research work. BM acknowledges the support of Anusandhan National Research Foundation(ANRF), Science & Engineering Research Board(SERB), DST for the grant (File No: CRG/2023/000475). The authors gratefully acknowledge the computing time provided on the high-performance computing facility, Sharanga, at the Birla Institute of Technology and Science - Pilani, Hyderabad Campus.

VII. REFERENCES

-
- [1] **Supernova Search Team** Collaboration, A. G. Riess *et al.*, "Observational evidence from supernovae for an accelerating universe and a cosmological constant," *Astron. J.* **116** (1998) 1009–1038, [arXiv:astro-ph/9805201](#).
 - [2] **Supernova Cosmology Project** Collaboration, S. Perlmutter *et al.*, "Measurements of Ω and Λ from 42 high redshift supernovae," *Astrophys. J.* **517** (1999) 565–586, [arXiv:astro-ph/9812133](#).
 - [3] C. L. Bennett and *et al.*, "First-Year Wilkinson Microwave Anisotropy Probe (WMAP)* Observations: Preliminary Maps and Basic Results," *The Astrophysical Journal Supplement Series* **148** (2003) no. 1, 1, [arXiv:astro-ph/0302207](#).
 - [4] M. Tegmark *et al.*, "Cosmological parameters from SDSS and WMAP," *Physical Review D* **69** (2004) no. 10, , [arXiv:astro-ph/0310723](#).
 - [5] S. Alam and *et al.*, "The clustering of galaxies in the completed SDSS-III Baryon Oscillation Spectroscopic Survey: cosmological analysis of the DR12 galaxy sample," *Monthly Notices of the Royal Astronomical Society* **470** (2017) no. 3, 2617–2652, [arXiv:1607.03155 \[astro-ph.CO\]](#).
 - [6] D. M. Scolnic *et al.*, "The Complete Light-curve Sample of Spectroscopically Confirmed SNe Ia from Pan-STARRS1 and Cosmological Constraints from the Combined Pantheon Sample," *The Astrophysical Journal* **859** (2018) no. 2, 101, [arXiv:1710.00845 \[astro-ph.CO\]](#).
 - [7] A. G. Riess, S. Casertano, W. Yuan, L. M. Macri, and D. Scolnic, "Large Magellanic Cloud Cepheid Standards Provide a 1% Foundation for the Determination of the Hubble Constant and Stronger Evidence for Physics beyond Λ CDM," *Astrophys. J.* **876** (2019) no. 1, 85, [arXiv:1903.07603 \[astro-ph.CO\]](#).
 - [8] D. Benisty and D. Staicova, "Testing late-time cosmic acceleration with uncorrelated baryon acoustic oscillation dataset," *Astronomy & Astrophysics* **647** (2021) A38, [arXiv:2009.10701 \[astro-ph.CO\]](#).
 - [9] **DES Collaboration** Collaboration, "Dark Energy Survey Year 3 results: calibration of lens sample redshift distributions using clustering redshifts with BOSS/eBOSS," *Monthly Notices of the Royal Astronomical Society* **513** (2022) no. 4, 5517–5539, [arXiv:2012.12826 \[astro-ph.CO\]](#). <http://dx.doi.org/10.1093/mnras/stac1160>.
 - [10] R. P. Gupta, "JWST early Universe observations and Λ CDM cosmology," *Monthly Notices of the Royal Astronomical Society* **524** (2023) no. 3, 3385–3395, [arXiv:2309.13100 \[astro-ph.CO\]](#).

- [11] **Planck Collaboration** Collaboration, “Planck2013 results. XVI. Cosmological parameters,” *Astronomy & Astrophysics* **571** (2014) A16, [arXiv:1303.5076 \[astro-ph.CO\]](#).
- [12] A. G. Riess *et al.*, “A Comprehensive Measurement of the Local Value of the Hubble Constant with $1 \text{ km s}^{-1} \text{ Mpc}^{-1}$ Uncertainty from the Hubble Space Telescope and the SH0ES Team,” *The Astrophysical Journal Letters* **934** (2022) no. 1, L7, [arXiv:2112.04510 \[astro-ph.CO\]](#).
- [13] Wang and *et al.*, “H0LiCOW XIII. A 2.4 % measurement of H_0 from lensed quasars: 5.3σ tension between early and late-Universe probes,” *Monthly Notices of the Royal Astronomical Society* **498** (2019) no. 1, 1420–1439, [arXiv:1907.04869 \[astro-ph.CO\]](#).
- [14] W. L. Freedman and *et al.*, “The Carnegie-Chicago Hubble Program. VIII. An Independent Determination of the Hubble Constant Based on the Tip of the Red Giant Branch*,” *The Astrophysical Journal* **882** (2019) no. 1, 34, [arXiv:1907.05922 \[astro-ph.CO\]](#).
- [15] **Planck** Collaboration, N. Aghanim *et al.*, “Planck 2018 results. VI. Cosmological parameters,” *Astron. Astrophys.* **641** (2020) A6, [arXiv:1807.06209 \[astro-ph.CO\]](#). [Erratum: *Astron. Astrophys.* 652, C4 (2021)].
- [16] **DES Collaboration** Collaboration, “Dark Energy Survey Year 1 Results: A Precise H_0 Estimate from DES Y1, BAO, and D/H Data,” *Monthly Notices of the Royal Astronomical Society* **480** (2018) no. 3, 3879–3888, [arXiv:1711.00403 \[astro-ph.CO\]](#).
- [17] E. Di Valentino, A. Melchiorri, and O. Mena, “Can interacting dark energy solve the H_0 tension?,” *Physical Review D* **96** (2017) no. 4, [arXiv:1704.08342 \[astro-ph.CO\]](#).
- [18] E. Di Valentino, O. Mena, S. Pan, L. Visinelli, W. Yang, A. Melchiorri, D. F. Mota, A. G. Riess, and J. Silk, “In the realm of the Hubble tension - a review of solutions,” *Classical and Quantum Gravity* **38** (2021) no. 15, 153001, [arXiv:2103.01183 \[astro-ph.CO\]](#).
- [19] S. Nojiri and S. D. Odintsov, “Modified $f(R)$ gravity consistent with realistic cosmology: From a matter dominated epoch to a dark energy universe,” *Phys. Rev. D* **74** (2006) 086005, [arXiv:hep-th/0608008](#).
- [20] S. Nojiri and S. D. Odintsov, “Unifying inflation with Λ CDM epoch in modified $f(R)$ gravity consistent with Solar System Test,” *Physics Letters B* **657** (2007) no. 4, 238–245, [arXiv:0707.1941 \[hep-th\]](#).
- [21] T. P. Sotiriou and V. Faraoni, “ $f(R)$ Theories Of Gravity,” *Rev. Mod. Phys.* **82** (2010) 451–497, [arXiv:0805.1726 \[gr-qc\]](#).
- [22] S. Capozziello and M. De Laurentis, “Extended Theories of Gravity,” *Phys. Rept.* **509** (2011) 167–321, [arXiv:1108.6266 \[gr-qc\]](#).
- [23] J. W. Maluf, “Hamiltonian formulation of the teleparallel description of general relativity,” *J. Math. Phys.* **35** (1994) 335–343, [arXiv:gr-qc/0002059](#).
- [24] R. Aldrovandi and J. G. Pereira, *Teleparallel Gravity: An Introduction*. Springer, 2013.
- [25] R. Weitzenböck, ‘Invariantentheorie’. Noordhoff, Gronningen, 1923.
- [26] G. R. Bengochea and R. Ferraro, “Dark torsion as the cosmic speed-up,” *Phys. Rev. D* **79** (2009) 124019, [arXiv:0812.1205 \[astro-ph\]](#).
- [27] R. Ferraro and F. Fiorini, “On Born-Infeld Gravity in Weitzenböck spacetime,” *Phys. Rev. D* **78** (2008) 124019, [arXiv:0812.1981 \[gr-qc\]](#).
- [28] E. V. Linder, “Einstein’s Other Gravity and the Acceleration of the Universe,” *Phys. Rev. D* **81** (2010) 127301, [arXiv:1005.3039 \[astro-ph.CO\]](#). [Erratum: *Phys. Rev. D* 82, 109902 (2010)].
- [29] S.-H. Chen, J. B. Dent, S. Dutta, and E. N. Saridakis, “Cosmological perturbations in $f(T)$ gravity,” *Phys. Rev. D* **83** (2011) 023508, [arXiv:1008.1250 \[astro-ph.CO\]](#).
- [30] Y.-F. Cai, S. Capozziello, M. D. Laurentis, and E. N. Saridakis, “ $f(T)$ teleparallel gravity and cosmology,” *Reports on Progress in Physics* **79** (2016) no. 10, 106901.
- [31] L. K. Duchaniya, S. V. Lohakare, B. Mishra, and S. K. Tripathy, “Dynamical stability analysis of accelerating $f(T)$ gravity models,” *Eur. Phys. J. C* **82** (2022) no. 5, 448, [arXiv:2202.08150 \[gr-qc\]](#).
- [32] R. Briffa, C. Escamilla-Rivera, J. Levi Said, and J. Mifsud, “Growth of structures using redshift space distortion in $f(T)$ cosmology,” *Monthly Notices of the Royal Astronomical Society* **528** (2024) no. 2, 2711–2727, [arXiv:2310.09159 \[gr-qc\]](#).
- [33] L. K. Duchaniya, K. Gandhi, and B. Mishra, “Attractor behavior of $f(T)$ modified gravity and the cosmic acceleration,” *Physics of the Dark Universe* **44** (2024) 101461, [arXiv:2303.09076 \[gr-qc\]](#).
- [34] G. Kofinas and E. N. Saridakis, “Teleparallel equivalent of Gauss-Bonnet gravity and its modifications,” *Phys. Rev. D* **90** (2014) 084044, [arXiv:1404.2249 \[gr-qc\]](#).
- [35] G. Kofinas and E. N. Saridakis, “Cosmological applications of $F(T, T_G)$ gravity,” *Phys. Rev. D* **90** (2014) 084045, [arXiv:1408.0107 \[gr-qc\]](#).
- [36] C. Escamilla-Rivera and J. Levi Said, “Cosmological viable models in $f(T, B)$ theory as solutions to the H_0 tension,” *Class. Quant. Grav.* **37** (2020) no. 16, 165002, [arXiv:1909.10328 \[gr-qc\]](#).
- [37] S. A. Kadam, N. P. Thakkar, and B. Mishra, “Dynamical system analysis in teleparallel gravity with boundary term,” *The European Physical Journal C* **83** (2023) no. 9, [arXiv:2306.06677 \[gr-qc\]](#).

- [38] M. Gonzalez-Espinoza and G. Otalora, "Cosmological dynamics of dark energy in scalar-torsion $f(T, \phi)$ gravity," *Eur. Phys. J. C* **81** (2021) no. 5, 480, [arXiv:2011.08377 \[gr-qc\]](#).
- [39] M. Gonzalez-Espinoza, G. Otalora, and J. Saavedra, "Stability of scalar perturbations in scalar-torsion $f(T, \phi)$ gravity theories in the presence of a matter fluid," *JCAP* **10** (2021) 007, [arXiv:2101.09123 \[gr-qc\]](#).
- [40] L. K. Duchaniya, B. Mishra, and J. L. Said, "Noether symmetry approach in scalar-torsion $f(T, \phi)$ gravity," *The European Physical Journal C* **83** (2023) no. 7, , [arXiv:2210.11944 \[gr-qc\]](#).
- [41] L. K. Duchaniya, S. A. Kadam, J. L. Said, and B. Mishra, "Dynamical systems analysis in $f(T, \phi)$ gravity," *The European Physical Journal C* **83** (2023) no. 1, , [arXiv:2209.03414 \[gr-qc\]](#).
- [42] T. Harko, F. S. Lobo, G. Otalora, and E. N. Saridakis, " $f(T, T)$ gravity and cosmology," *Journal of Cosmology and Astroparticle Physics* **2014** (2014) no. 12, 021, [arXiv:1405.0519 \[gr-qc\]](#).
- [43] D. Momeni and R. Myrzakulov, "Cosmological reconstruction of $f(T, T)$ gravity," *International Journal of Geometric Methods in Modern Physics* **11** (2014) no. 08, 1450077, [arXiv:1405.5863 \[gr-qc\]](#).
- [44] G. Farrugia and J. L. Said, "Growth factor in $f(T, T)$ gravity," *Phys. Rev. D* **94** (2016) 124004, [arXiv:1612.00974 \[gr-qc\]](#).
- [45] E. L. B. Junior, M. E. Rodrigues, I. G. Salako, and M. J. S. Houndjo, "Reconstruction, thermodynamics and stability of the Λ CDM model in $f(T, T)$ gravity," *Classical and Quantum Gravity* **33** (2016) no. 12, 125006, [arXiv:1501.00621 \[gr-qc\]](#).
- [46] M. Pace and J. L. Said, "Quark Stars in $f(T, T)$ -Gravity," *The European Physical Journal C* **77** (2017) no. 2, , [arXiv:1701.04761 \[gr-qc\]](#).
- [47] L. K. Duchaniya, S. V. Lohakare, and B. Mishra, "Cosmological models in $f(T, T)$ gravity and the dynamical system analysis," *Physics of the Dark Universe* **43** (2024) 101402, [arXiv:2302.07132 \[gr-qc\]](#).
- [48] W. L. Freedman, "Measurements of the hubble constant: Tensions in perspective," *The Astrophysical Journal* **919** (2021) no. 1, 16, [arXiv:2106.15656 \[astro-ph\]](#). <http://dx.doi.org/10.3847/1538-4357/ac0e95>.
- [49] E. Abdalla and et all, "Cosmology intertwined: A review of the particle physics, astrophysics, and cosmology associated with the cosmological tensions and anomalies," *Journal of High Energy Astrophysics* **34** (2022) 49–211, [arXiv:2203.06142 \[astro-ph.CO\]](#).
- [50] M. Moresco and et al., "Unveiling the universe with emerging cosmological probes," *Living Reviews in Relativity* **25** (2022) no. 1, , [arXiv:2201.07241 \[astro-ph.CO\]](#).
- [51] D. Brout and et al., "The Pantheon+ Analysis: Cosmological Constraints," *The Astrophysical Journal* **938** (2022) no. 2, 110, [arXiv:2202.04077 \[astro-ph.CO\]](#).
- [52] R. Briffa, C. Escamilla-Rivera, J. L. Said, J. Mifsud, and N. L. Pullicino, "Impact of H_0 priors on $f(T)$ late time cosmology," *The European Physical Journal Plus* **137** (2022) no. 5, , [arXiv:2108.03853 \[astro-ph.CO\]](#).
- [53] S. Vagnozzi, "Seven Hints That Early-Time New Physics Alone Is Not Sufficient to Solve the Hubble Tension," *Universe* **9** (2023) no. 9, 393, [arXiv:2308.16628 \[astro-ph.CO\]](#).
- [54] S. Capozziello, G. Sarracino, and G. De Somma, "A Critical Discussion on the H_0 Tension," *Universe* **10** (2024) no. 3, 140, [arXiv:2403.12796 \[gr-qc\]](#).
- [55] C. Misner, K. Thorne, and J. Wheeler, *Gravitation*. No. pt. 3 in Gravitation. W. H. Freeman, 1973. <https://books.google.com.mt/books?id=w4Gigq3tY1kC>.
- [56] D. Foreman-Mackey, D. W. Hogg, D. Lang, and J. Goodman, "emcee: The mcmc hammer," *Publications of the Astronomical Society of the Pacific* **125** (2013) no. 925, 306–312, [arXiv:1202.3665 \[astro-ph.CO\]](#).
- [57] R. Jimenez and A. Loeb, "Constraining cosmological parameters based on relative galaxy ages," *The Astrophysical Journal* **573** (2002) no. 1, 37–42, [arXiv:astro-ph/0106145 \[astro-ph.CO\]](#).
- [58] Z. Cong, Z. Han, Y. Shuo, L. Siqu, Z. Tong-Jie, and S. Yan-Chun, "Four new observational $H(z)$ data from luminous red galaxies in the Sloan Digital Sky Survey data release seven," *Research in Astronomy and Astrophysics* **14** (2014) no. 10, 1221, [arXiv:1207.4541 \[astro-ph.CO\]](#). <https://dx.doi.org/10.1088/1674-4527/14/10/002>.
- [59] R. Jimenez, L. Verde, T. Treu, and D. Stern, "Constraints on the Equation of State of Dark Energy and the Hubble Constant from Stellar Ages and the Cosmic Microwave Background," *The Astrophysical Journal* **593** (2003) no. 2, 622–629, [arXiv:astro-ph/0302560 \[astro-ph.CO\]](#).
- [60] M. Moresco and et al., "A 6% measurement of the Hubble parameter at $z \sim 0.45$: direct evidence of the epoch of cosmic re-acceleration," *Journal of Cosmology and Astroparticle Physics* **2016** (2016) no. 05, 014–014, [arXiv:1601.01701 \[astro-ph.CO\]](#).
- [61] J. Simon, L. Verde, and R. Jimenez, "Constraints on the redshift dependence of the dark energy potential," *Physical Review D* **71** (2005) no. 12, , [arXiv:astro-ph/0412269 \[astro-ph.CO\]](#).
- [62] M. Moresco and et al., "Improved constraints on the expansion rate of the Universe up to $z \sim 1.1$ from the spectroscopic evolution of cosmic chronometers," *Journal of Cosmology and Astroparticle Physics* **2012** (2012) no. 08, 006–006, [arXiv:1201.3609 \[astro-ph.CO\]](#).
- [63] D. Stern, R. Jimenez, L. Verde, M. Kamionkowski, and S. A. Stanford, "Cosmic chronometers: constraining the equation of state of dark energy. I: $H(z)$ measurements," *Journal of Cosmology and Astroparticle Physics* **2010** (2010) no. 02, 008–008,

[arXiv:0907.3149](#) [[astro-ph.CO](#)].

- [64] M. Moresco, "Raising the bar: new constraints on the Hubble parameter with cosmic chronometers at $z \sim 2$," *Monthly Notices of the Royal Astronomical Society* **450** (2015) no. 1, 16–20, [arXiv:1503.01116](#) [[astro-ph.CO](#)].
- [65] D. Brout and et al., "The Pantheon+ Analysis: SuperCal-fragilistic Cross Calibration, Retrained SALT2 Light-curve Model, and Calibration Systematic Uncertainty," *The Astrophysical Journal* **938** (2022) no. 2, 111, [arXiv:2112.03864](#) [[astro-ph.CO](#)].
- [66] D. Scolnic and et al., "The Pantheon+ Analysis: The Full Data Set and Light-curve Release," *The Astrophysical Journal* **938** (2022) no. 2, 113, [arXiv:2112.03863](#) [[astro-ph.CO](#)].
- [67] A. Conley and et al., "Supernova constraints and systematic uncertainties from the first three years of the supernova legacy survey," *The Astrophysical Journal Supplement Series* **192** (2010) no. 1, 1, [arXiv:1104.1443](#) [[astro-ph.CO](#)].
- [68] F. Beutler and et al., "The 6dF Galaxy Survey: baryon acoustic oscillations and the local Hubble constant: 6dFGS: BAOs and the local Hubble constant," *Monthly Notices of the Royal Astronomical Society* **416** (2011) no. 4, 3017–3032, [arXiv:1106.3366](#) [[astro-ph.CO](#)].
- [69] H. du Mas des Bourboux and et al., "Baryon acoustic oscillations from the complete SDSS-III Ly α -quasar cross-correlation function at $z = 2.4$," *Astronomy & Astrophysics* **608** (2017) A130, [arXiv:1708.02225](#) [[astro-ph.CO](#)].
- [70] A. J. Ross and et al., "The clustering of the SDSS DR7 main Galaxy sample I. A 4 per cent distance measure at $z=0.15$," *Monthly Notices of the Royal Astronomical Society* **449** (2015) no. 1, 835–847, [arXiv:1409.3242](#) [[astro-ph.CO](#)].
- [71] G.-B. Zhao and et al., "The clustering of the sdss-iv extended baryon oscillation spectroscopic survey dr14 quasar sample: a tomographic measurement of cosmic structure growth and expansion rate based on optimal redshift weights," *Monthly Notices of the Royal Astronomical Society* **482** (2018) no. 3, 3497–3513, [arXiv:1801.03043](#) [[astro-ph.CO](#)].
- [72] D. J. Fixsen, "The temperature of the cosmic microwave background," *The Astrophysical Journal* **707** (2009) no. 2, 916–920, [arXiv:0911.1955](#) [[astro-ph.CO](#)].
- [73] S. Capozziello, O. Farooq, O. Luongo, and B. Ratra, "Cosmographic bounds on the cosmological deceleration-acceleration transition redshift in $f(\mathcal{R})$ gravity," *Phys. Rev. D* **90** (2014) 044016, [arXiv:1403.1421](#) [[gr-qc](#)].
- [74] D. Camarena and V. Marra, "Local determination of the hubble constant and the deceleration parameter," *Phys. Rev. Res.* **2** (2020) 013028, [arXiv:1906.11814](#) [[astro-ph.CO](#)].
- [75] V. Sahni, A. Shafieloo, and A. A. Starobinsky, "Two new diagnostics of dark energy," *Phys. Rev. D* **78** (2008) 103502, [arXiv:0807.3548](#) [[astro-ph.CO](#)].
- [76] V. Sahni, T. D. Saini, A. A. Starobinsky, and U. Alam, "Statefinder-a new geometrical diagnostic of dark energy," *Journal of Experimental and Theoretical Physics Letters* **77** (2003) no. 5, 201–206, [arXiv:astro-ph/0201498](#) [[astro-ph.CO](#)].